Interactions Between Tectonic Deformation and Erosion During the Seismic Cycle in Mountain Ranges

Philippe Steer

Chapitre X

Interactions between tectonic deformation and erosion during the seismic cycle in mountain ranges

Introduction

The topography of mountain ranges is the result of a competition, integrated over time, between tectonic uplift and erosion processes. For example, a topography under construction will have uplift rates greater than rates of erosion, while a declining topography will have erosion greater than uplift rates. However, rates of erosion and uplift do not evolve strictly independently. On geologic time scales (>100 kyr), uplift allows for an increase in topography relief and slopes, which in turn increases erosion rates. This reflects the "action" of tectonics on erosion and is explained in particular by the high sensitivity of river (e.g. incision) and hillslope (e.g. landslides) erosion processes to gravity and thus to slope (e.g. Ahnert, 1970; Bonnet & Crave, 2003). In addition, many studies suggest a "feedback" effect of erosion on tectonics, notably through isostasy and through the modification of the stress tensor resulting from erosion-induced topographic unloading (e.g. Willett et al., 1999; Vernant et al., 2013; Thieulot et al., 2014). These principles of action and feedback, between tectonic and erosion processes, favour the development of a dynamic balance between uplift and erosion rates (Gilbert, 1877; Whipple, 2009). A corollary feature of this dynamic equilibrium is a state characterised by a constant mean-elevation topography that can be sustained on geological time scales. The foundations of modern quantitative geomorphology have thus been built around this paradigm of steady state landscapes responding to progressive changes in climatic or tectonic conditions (e.g. Whipple & Tucker, 1999, 2002). In the last decades, numerous studies have used this idea to explore the long-term signature of climate and tectonics in landscape form (e.g. Kirby & Whipple, 2012; Willett et al., 2014).

However, this view is challenged by the observation of landscape dynamics at the scale of the seismic cycle (<1 kyr). While mountain landscapes are the result of a long geological history, their dynamics are marked by a series of discrete and potentially extreme disturbances during earthquakes or storms (Dadson et al., 2003; Lague et al., 2005; Parker et al., 2011; Hovius et al., 2011). During these events, elementary geomorphic processes become active and are catalysed by the disturbances. For example, in August 2009 Typhoon Morakot generated up to 3 m of rain in Taiwan in 3 days, triggered more than 10,000 landslides (Lin et al., 2011; Marc et al., 2018) and led to a large increase in sedimentary flows (Huang & Montgomery, 2013). This discrete erosion event could correspond to 10 to 100 years of erosion at the 10-year average rate (Dadson et al., 2003). Large magnitude earthquakes represent a second type of landscape disturbance, as evidenced by the ~200,000 landslides potentially induced by the 2008 Wenchuan (China) earthquake of magnitude Mw 7.9 (Parker et al., 2011; Li et al., 2014; Fan et al., 2018). It is even suggested that the total volume of landslides produced during such an earthquake could equal or even exceed the volume of uplifted rock resulting from co-seismic displacement (Parker et al., 2011; Marc et al., 2016; Li et al., 2019).

In addition, these elementary processes occur in chains or cascades of events, resulting in major changes in the mechanical properties of hillslopes, the rate of landslides (Keefer, 1984; Malamud et al., 2004; Marc et al., 2015), the rate of rock alteration (Emberson et al, 2016), inorganic (Hovius et al., 2011; Croissant et al., 2017a) and organic (Hilton et al., 2008; Frith et al., 2018) sediment fluxes, river morphology (Yanites et al., 2010; Croissant et al., 2017b) and hydrological and hydrogeological flows (Montgomery & Manga, 2003; Mohr et al., 2017). These rapid erosion events in turn induce potential feedbacks with tectonic and even seismic activity (Calais et al., 2010; Steer et al., 2014; Steer et al., 2020). Such elementary processes and chains of events, on a short time scale, are currently not taken into account by numerical models studying the evolution of mountain landscapes (e.g., Tucker et al., 2001; Crave and Davy, 2001; Braun and Willett, 2013; Campforts et al., 2017). As a result, we do not know what the impact of these extreme events is on landscape form and dynamics, whether steady-state can be maintained following these disturbances (Peizhen et al., 2001; Finnegan et al., 2014) or how to interpret landscape form in terms of the frequency and magnitude of these disturbances, which are the cause of major natural disasters.

In this section, we will first present a current synthetic view on landscape dynamics based on the paradigm of landscapes reaching a state of dynamic equilibrium. We will then attempt to present the results and evidence from field observations, satellite and geophysical imagery, and numerical simulations challenging this paradigm and supporting the idea of landscapes constantly disturbed

by extreme events, especially during the seismic cycle. We will focus on the impact of earthquakes on landscapes through the triggering of numerous landslides during the co-seismic phase. These landslides being the starting point of many secondary geomorphological processes, we will try to understand the link between the number or volume of these landslides and the characteristics of the earthquake and the impacted topography. Then, we will describe the evolution of these landslides and disturbed landscapes during the post-seismic relaxation phase of the topography. This will allow us to quantify the topographic balance of the seismic cycle. This article is mainly a non-exhaustive synthesis of the existing literature on the subject with choices of works and interpretations sometimes personal or subjective.

2.1. The Paradigm of steady-state landscapes

In ice-free landscapes, the evolution of continental landforms on large time scales (> 10 kyr) is generally described by a competition between tectonic uplift and erosion of rivers and hillslopes. In the absence of sedimentation, the evolution of topographic height h is thus controlled by the imbalance between the topographic uplift rate U and the erosion rate E:

$$\frac{\partial h}{\partial t} = U - E \qquad [2.1]$$

In its simplest formulation, it is proposed that the rate of river erosion E is a function of the local slope S and the specific river discharge Q_w, and thus of the precipitation P:

$$E = K{Q_w}^m S^n, \qquad [2.2]$$

where K is a coefficient of erosion efficiency, which depends on river bed lithology and sediment discharge, among other factors, and m and n are positive exponents (Howard and Kerby, 1983; Howard et al., 1994; Whipple & Tucker, 1999; Lague et al., 2014). The m/n ratio, called the concavity index, should be close to 0.5 based on river profile geometry, and the pair $m = 0.5$ and $n = 1$ is often chosen for non-alluvial rivers. In the simple modelling approach that we develop here, hydrological flows at the surface of the topography, resulting from precipitation P, are routed gradually in the direction of the steepest slope until they reach an outlet. Slope dynamics are generally modelled either by a diffusion law or by a maximum threshold on the local slope corresponding to the resting slope beyond which gravitational movements are activated. In the following, we will consider the latter approach by setting the maximum slope at 30°. Numerically, equation 2 is solved by an implicit scheme with the finite difference method (Braun & Willett, 2013).

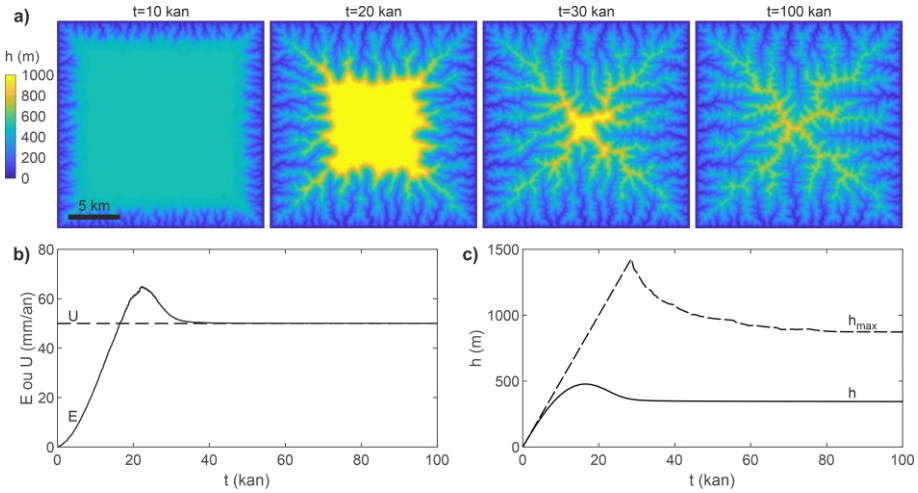

Figure 2.1. *a) Maps of the temporal evolution of the topography h of a relief subject to tectonic uplift and erosion by rivers and slopes. b) Temporal evolution of the rates of uplift U and erosion E averaged over the whole model. c) Temporal evolution of the mean elevation h and maximum elevation h_{max} of the topography. Erosion rates higher than the uplift rate are obtained around 20 kyr and are explained in particular by a transient imbalance of the planar hydrological flow network during the incision of the plateau (e.g. Carretier et al., 2009).*

In the presence of a uniform uplift rate combined with a constant base level, such a system of equations results in the progressive building of relief (see Figure 2.1). The initial plateau is first incised at its edges, following the initiation of uplift (see Figure 2.1a). Rivers associated with preferential flows quickly emerge and favour the propagation of the regressive erosion wave from downstream to upstream. Following the dissection of these valleys, the hillslopes gradually increase their slopes until they reach the angle of repose. The increase in the slopes of the hillslopes and rivers leads to an erosion rate increase, which is then balanced with the uplift rate (see Figure 2.1b). The resulting relief and topography reach a dynamic steady-state (see Figure 2.1c). This dynamic steady-state can be maintained as long as the boundary conditions of the model, including its base level, uplift rates and precipitation rates, remain unchanged.

Any disturbance of these boundary conditions leads to a transtient phase of rebalancing of the relief with the new boundary conditions. The duration of this transient phase :

$$\tau = \beta U^{\frac{1}{n}-1} P^{-\frac{m}{n}} \quad [2.3]$$

is a function of the precipitation rate P and the uplift rate U, with a proportionality constant β which depends, among other things, on the characteristic size of the catchment areas and K (Whipple & Tucker, 1999). In the example model, the duration of this transitional phase is several tens of thousands of years (see Figure 2.1b,c). In active orogens such as Taiwan, the duration of this transient phase is probably on the order of one million years (Whipple, 2001). This transient phase is therefore much longer than the classical duration of a seismic cycle, about 50 to 1000 years, and even longer than the periodicity of some climatic cycles, such as those referred to as Milanković periodicities.

2.2. Earthquakes and co-seismic landslides

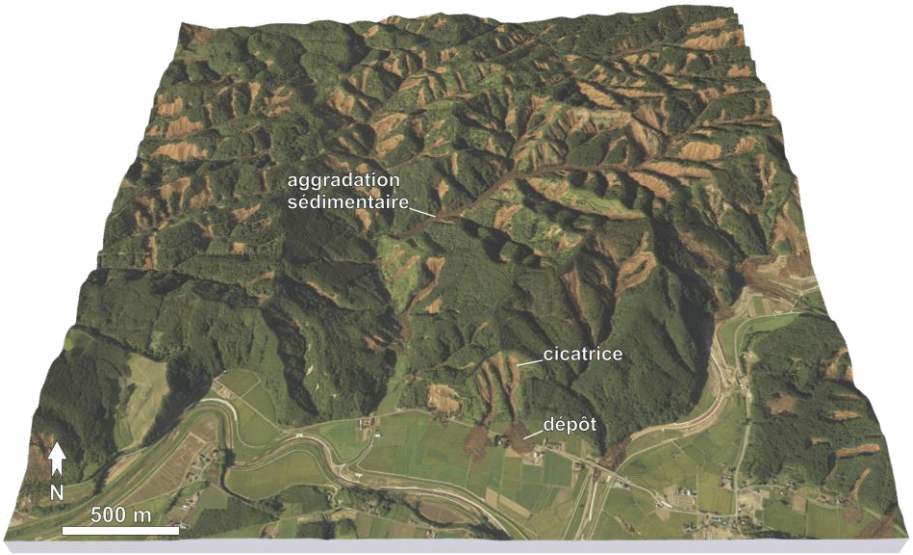

Figure 2.2. *3D block representing the epicentral zone of the Hokkaido (Japan) earthquake of magnitude 6.6, which took place on September 6, 2018, where numerous co-seismic landslides were observed. Landslide scars, depositional zones and sedimentary aggregation in the valleys are visible in this figure. A satellite image is draped over the topography. Source :*

https://maps.gsi.go.jp/#16/42.766793/141.962703/&base=std&ls=std%7C20180906hokkaido_atsuma_0906do&blend=0&disp=11&lcd=20180906hokkaido_atsumachiku_0906suichoku&vs=c0j0h0k0l0u0t0z0r0s1m0f0&vs2=f0&sync=1&base2=ort&ls2=ort%7Cexperimental_anno&disp2=11&reliefdata=0G000000.

This simplistic view of the long-term dynamics (> 10 kyr) of continental landscapes neglects, however, many processes and forcings generating perturbations on shorter time scales (Dadson et al., 2004). For example, numerous studies have demonstrated the significant role of earthquakes on landscape dynamics (Keefer, 1984; Hovius, 2011; Parker et al., 2011; Li et al., 2014; Marc et al., 2016a,b). Large magnitude earthquakes (see Figure 2.2), such as the 7.9 magnitude Wenchuan earthquake in 2008, are capable of potentially triggering up to several hundred thousand landslides in the vicinity of the fault that ruptured during the earthquake (Li et al., 2014; Fan et al., 2018). In terms of order of magnitude, the mass of sediment produced by landslides during the Wenchuan earthquake, ~7.4 Gt (Zhang et al., 2019), represents ~40% of the annual global sediment flow from the continents to the ocean, or 19 Gt (Milliman & Farnsworth, 2013). In addition to this earthquake, two other events mentioned by Hovius et al. (2011) provide insight into the erosive potential of earthquakes: 1) the Assam 8.6 magnitude earthquake in 1950 possibly triggered a total landslide volume close to 47 km^3 , with a total mass close to ~120 Gt (Mathur, 1953) and; 2) the 7.9 magnitude earthquake in Papua New Guinea in 1937 potentially caused between 74 and 400 mm of erosion (Simonett, 1967). These co-seismic landslides include both shallow landslides, deep-seated landslides, rockfalls and avalanches. The initiation of co-seismic landslides is generally attributed to the passage of seismic waves, and in particular to the peak ground acceleration (PGA) associated with volume waves. In addition to physical predictions (e.g. Newmark, 1965), this inference is consistent with the observation of a spatial correlation between PGA and landslide spatial density (Meunier et al., 2007). However, the triggering mechanism is subject to debate, and some authors observe an influence of the distance to the fault (Massey et al., 2018) or of the maximum speed of displacements induced by the passage of seismic waves.

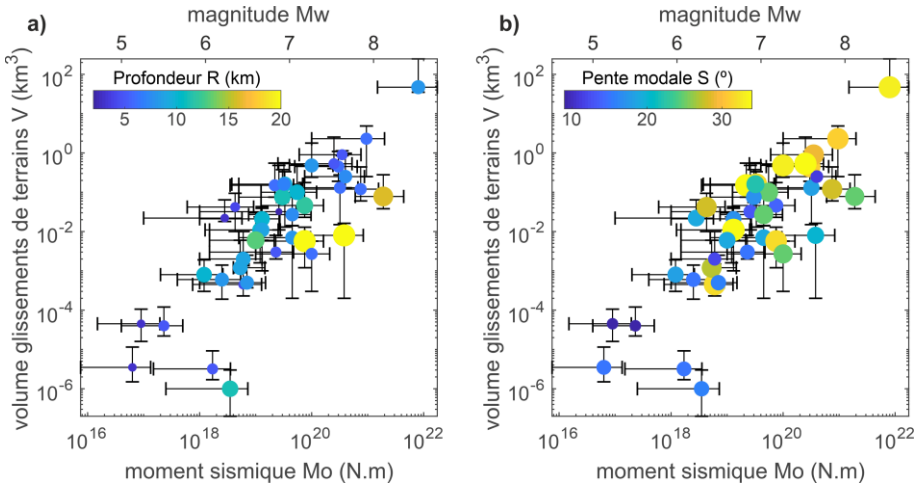

Figure 2.3. *a) Influence of the magnitude M_W, the seismic moment M_0 and the depth of an earthquake R on the volume V of co-seismic landslides. b) Influence of the modal slope S of the topography of the epicentral zone on the volume V of co-seismic landslides. Modified from Marc et al (2016)a.*

The development of satellite imagery, especially at high resolution (~1 m), has led to numerous inventories of landslides triggered by earthquakes (Tanyas et al., 2017) or intense rainfall events (Marc et al., 2018). These inventories provide a better understanding of the characteristics of earthquakes that trigger numerous landslides (Marc et al., 2016a,b). First, the seismic moment M_0 or the magnitude of the earthquakes:

$$M_W = \frac{2}{3}\log_{10}(M_0) - 6.07 \qquad [2.4]$$

emerges empirically as the predominant factor controlling the total volume V of co-seismic landslides (Keefer, 1984; Keefer, 1999; Marc et al., 2016a,b). Below a magnitude threshold close to 5, earthquakes are no longer able to generate a sufficiently large PGA, greater than ~0.2 g, to trigger a significant number of landslides. Above a magnitude of ~5, it is empirically observed that PGA increases exponentially with the seismic moment until it saturates beyond a magnitude of ~7 (Boore & Atkinson, 2008). Combined with the increase in fault rupture length with seismic moment (Leonard, 2010) and thus of the surface area of the landscape subjected to high PGA, it is observed that V increases more than linearly with M_0 (see Figure 2.2) (Marc et al., 2016a). For magnitudes greater than ~7, the increase in V

with M_0 is only allowed to be due to the increase in the length of the fault rupture with M0. Second, the depth R of the earthquakes also has a fundamental impact on the number of co-seismic landslides and on V. Indeed, the deeper the seismic rupture, the lower the acceleration induced by the surface seismic waves will be. This directly results from the attenuation of the seismic waves during their geometric propagation and by possible inelastic or dispersion effects. Third, the presence of slopes close to mechanical instability in the epicentral zone favours the number of landslides.

However, this empirical view of the role of the magnitude and depth of the earthquake and the slope of the reliefs on the triggering of landslides would deserve to be confronted with a physical modelling of these processes. Indeed, the propensity of a slope to generate a landslide is conditioned, among other things, by the mechanical state of the rocks composing it, inherited from the geological nature of the rocks and the deformations and fatigue processes expressed over geological time, by the shape of the slope, inherited from a morphological history over several thousand years, and from a hydrogeological state, developed over the previous months and years. For example, the Hokkaido (Japan) earthquake of magnitude 6.6, which occurred on 6 September 2018, triggered about 6,000 landslides (see Figure 2.2), while the earthquake nucleated at a depth of 37 km (Yamagishi & Yamazaki, 2018; Zhang et al., 2019). Such a depth is empirically considered to be unsuitable for the initiation of so many landslides. This being said, 1) the volcanic nature of the rocks with the presence of pumice stones at the base of the landslide surfaces, having a low threshold of resistance to mechanical shear and liquefaction (Li et al., 2020), 2) the possible saturation of the soils induced by the accumulation of 200 to 300 mm of precipitation during the previous month (Zhang et al, 2019) and 3) the occurrence of the Jebi supertyphoon, 1 day before the earthquake, associated with a significant atmospheric depression and less than 20 mm of precipitation, are all elements that placed the slopes of the epicentral zone close to a critical mechanical state even before the earthquake occurred..

2.3. Landslide size distributions

Earthquakes trigger landslides, the number and total volume of which vary greatly from one event to another. However, it is noteworthy that all these landslides follow a common distribution law of landslide size (see Figure 2.4). This distribution is characterized by a negative power distribution for landslides of intermediate to large size, and an exponential rollover for smaller landslides (Stark & Hovius, 2001; Guzzetti et al., 2002). This type of distribution can be approximated by an inverse-gamma (Malamud et al., 2004) or double-Paretto distribution. The size of landslides is currently characterized by the planar surface of the landslide, which can be

systematically measured, notably thanks to the contribution of high-resolution satellite images (e.g. Marc & Hovius, 2015; Massey et al., 2018). The volume of landslides is then generally obtained using empirical scaling laws with their area (Larsen et al., 2010). More recent work (e.g. Bernard et al., 2020) extends this approach to the volume of landslides through a pre- and post-earthquake comparison of high-resolution topographic data (e.g. Lidar). In all cases, a power law emerges from surface or volume-based distributions of landslides (Bernard et al., 2020). This raises the question of the mechanical and topographic properties of the slopes allowing the universal emergence of this power law. This is all the more motivated 1) by the consequences of such a distribution on the topographic impact of earthquakes (Parker et al., 2011: Marc et al., 2016b), 2) by the changes in hazard and risk induced by deviation from this law, and 3) by the observation that other physical processes and mechanical instabilities, such as earthquakes, respond to distribution laws of similar size or magnitude.

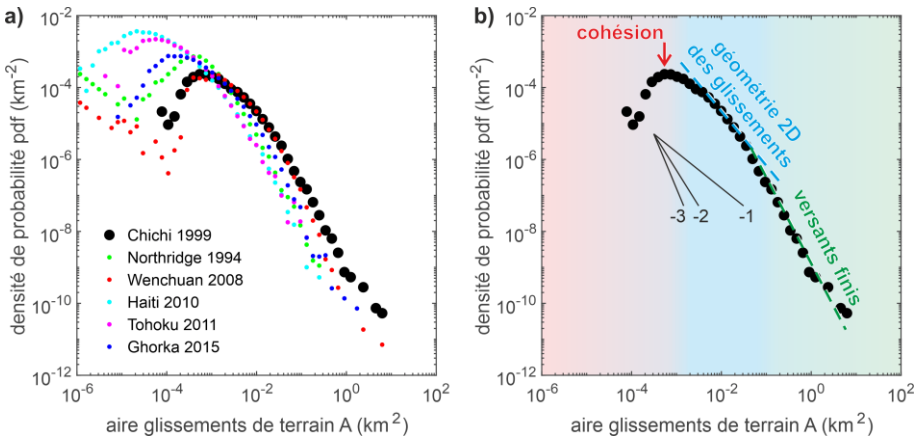

Figure 2.4. *Landslide size distribution. a) Probability densities of landslide areas from several co-seismic landslide inventories (Tanyas et al, (b) According to Jeandet et al. (2019), the rollover of the distribution (small sizes) is associated with the role of cohesion, the power law behaviour (intermediate sizes) is related to the presence of a scale law between landslide depth and area, and the deviation of the power law (large sizes) can be explained by a finite slope size effect.*

While the size distribution law of landslides is considered a universal property of landscapes (Malamud et al., 2004), the origin of the power law behaviour and its variability, with an exponent between -1.42 and -3.36 (Van Den Eeckhaut et al., 2007), remain open questions (see figure 2.4a). Similarly, the conditions allowing the existence of a rollover and the variability of its position, between ~10 and ~1000 m^2,

are debated (Tebbens, 2020). Reasons given for the under-representation of small landslides include 1) detectability due to the resolution of satellite images (Stark & Hovius, 2001), 2) amalgamation of small landslides (Tanyas et al., 2019), 3) or even satellite coverage too widely spaced in time (Barlow et al., 2012; Williams et al., 2018).

To explain the shape of landslide size distribution, Jeandet et al. (2019) propose a novel probabilistic model, integrating a criterion of mechanical strength of slopes and a topographic criterion, which we summarize here (see Figure 2.4b). In this model, the mechanical resistance of hillslopes is inferred from a Mohr-Coulomb criterion, integrating a slope cohesion C and a friction coefficient μ, applied to a potential rupture plane. The safety factor:

$$F = \frac{C+\mu\sigma_n}{\tau} \quad [2.5]$$

of such a plane is the ratio between the mechanical resistance, with σ_n the normal stress, and the driving stress, here the tangential stress τ induced by the potential landslide weight force. A point of the topography is considered unstable if it is associated with at least one potential failure plane 1) that intersects downstream the surface of the hillslope upstream of the river and 2) whose safety factor is unstable $F<1$. In addition to the above parameters, the depth of the plane and its dip appear to be two essential factors favouring gravitational instability.

This model naturally predicts the occurrence of a rollover for small landslide sizes, due to the dominant role of cohesion relative to friction for shallow depths. Beyond a certain depth, cohesion becomes negligible and the safety factor can be approximated by $\mu\sigma_n/\tau$, which becomes relatively invariant with depth as τ and σ_n are proportional. Thus, landslides of intermediate size have the same probability of failing. The probabilistic model, by considering a sampling without replacement (i.e. a large landslide prevents the occurrence of several smaller landslides) naturally leads to a power law behaviour for the landslide size distribution. This is referred to as self-similar statistical behaviour. The exponent of the power law is directly related to the scaling law between depth and area of landslides. For large landslides, i.e. those close to the size of the hillslope considered, the probability of failure is limited by the topographic criterion. This criterion is unfavourable for large landslides associated with too deep or too steep failure planes, with little chance of intersecting the hillslope upstream of the river. For natural landscapes, this finite size effect is of course subject to great variability due to the variability of hillslope lengths and heights. It promotes a deviation in power law behaviour for large landslides and imposes a maximum potential landslide size for a given landscape.

Thus, Jeandet et al (2019) offer a single relatively simple and mechanical-based model to explain the whole spectrum of landslide size distribution. As the total volume of triggered landslides is strongly dependent on the volume of the largest landslides, the model developed by Jeandet et al. (2019) highlights the predominant role of hillslope size in the topographic impact of large magnitude earthquakes. Moreover, apart from the role of cohesion, this model presents a certain similarity with the probabilistic models explaining the magnitude distribution of earthquakes (Jeandet, 2018). Indeed, it is generally proposed that the exponent (b-value) of the Gutenberg-Richter's law emerges from the scaling law relating the seismic moment of earthquakes to the area and displacement of earthquake ruptures. Moreover, finite size effects, controlled here by the depth of the seismogenic zone or by the size distribution of faults in a medium, could lead to a deviation of the distribution and limit the maximum magnitude allowed on a fault (Scholz, 1997).

2.4. Post-seismic relaxation of landscapes

Co-seismic landslides have a geomorphological impact that goes beyond the co-seismic phase. Indeed, sediments mobilized by landslides and reaching rivers or redepositing on hillslopes can generate sedimentary disturbances over the entire watersheds of the epicentral zone. This disturbance is characterised in particular by an increase in sediment discharge downstream of the landslides and by a phase of sediment aggregation in the valleys. The Chi-Chi earthquake of M_w 7.6 in Taiwan in 1999, which triggered more than 20,000 landslides in the epicentral zone, provided a well-documented case study thanks to a dense network of hydrological and sediment gauging stations (Dadson et al., 2003; Dadson et al., 2004). Following the Chi-Chi earthquake, measured concentrations of suspended sediments in rivers downstream of the epicentral zone increased by up to a factor of ~5 in the Choshui River watershed (Hovius et al., 2011). This positive anomaly of suspended sediment discharge fades over a period of about 6 years until it reaches the pre-Chi-Chi “background” sediment discharge. This 6-year period constrains a phase of post-seismic geomorphological relaxation of the landscapes, by analogy with the post-seismic geodynamic phase of the seismic cycle. This post-seismic phase does not allow the evacuation of all the sediments resulting from co-seismic landslides, but it does allow a return to a form of equilibrium in terms of sediment transport.

The duration of this post-seismic relaxation phase of the landscapes seems to present a certain variability. A duration close to 6 years is also deduced from measurements of suspended sediment concentration (less than 0.25 mm in diameter) after the Wenchuan earthquake (Wang et al., 2015). Similar values are obtained using post-seismic dilution of the detrital cosmogenic signal for larger sediments between

0.25 and 1 mm in size (West et al., 2014; Wang et al., 2017). The distal sedimentary deposits of the Zingpu Reservoir, downstream of the epicentral zone of the Wenchuan earthquake, recorded an increase in median particle size from 8 to 12-24 μm for ~6 years, starting 2 years after the earthquake (Zhang et al., 2019). However, Howarth et al. (2012, 2014) suggest a relaxation time of around 50 years from measurements of sediment cores obtained from two lakes near the Alpine Fault in New Zealand. It is also important to note that the post-seismic sediment fluxes associated with coarser grain sizes and transport modes are currently poorly known. However, this particle size represents a non-negligible part, possibly 10 to 90% by mass (e.g., Dadson et al., 2003; Fei, personal communication), of the sediments mobilised following an earthquake. Furthermore, while sediment discharge offers the advantage of providing a quantitative and integrative measure, it does not allow to discriminate between the processes at work during the post-earthquake phase.

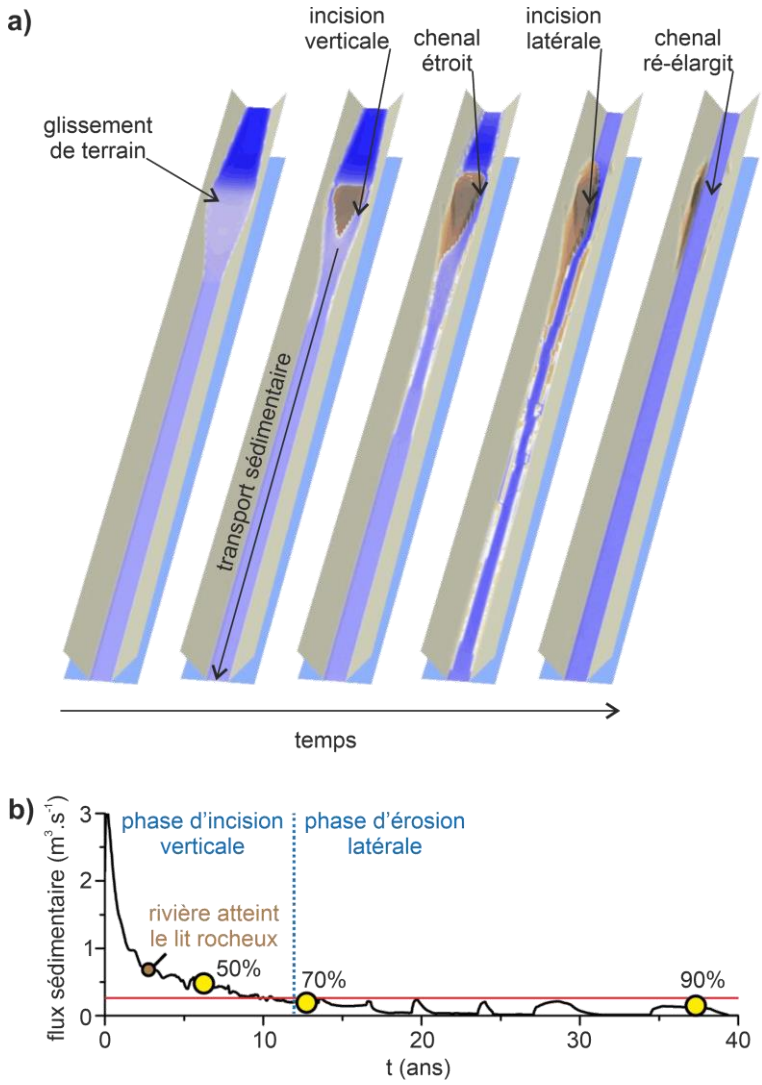

Figure 2.5. *Numerical modelling of the temporal evolution of a bedrock river located in a confined gorge following the deposition of a landslide, modified from Croissant et al (2017a). The numerical model used, Eros, includes the 2D resolution of hydraulic flows, vertical and lateral erosion and sediment transport (Davy et al., 2017). a) The scenario considered is that of a large volume landslide depositing in a river with a low sediment transport capacity. The river (in blue) first forms a dam lake upstream of the landslide and then vertically reincises the sediments (in brown) from the landslide. This rapid incision phase is associated with a very efficient sediment transport due to the reduction of the active channel width and the increase in the transport capacity of*

the river. This is followed by a slower phase of lateral erosion, leading to a progressive re-widening of the active channel and a less intense sediment transport, until the channel regains its initial geometry. b) Temporal evolution of the sediment discharge resulting from the landslide and measured downstream of the landslide in the river. The yellow dots indicate the percentage of the initial mass of the landslide that has been evacuated. The red line indicates the initial transport capacity of the river.

Conceptual, experimental, and numerical models thus offer a relevant tool to better understand the dynamics of the post-seismic geomorphological phase. Yanites et al (2010) develop a conceptual model to constrain the transport of the mass M of the sediment pulse delivered by co-seismic landslides. In this approach, the river, which is assumed to maintain its sediment transport capacity Q_T, exports away the sediment pulse in a time:

$$t = M/Q_T \quad [2.6]$$

For the Peikang River in Taiwan, which drains the epicentral zone of the Chi-Chi earthquake, the evacuation time is several tens to hundreds of years and thus potentially greater than or equal to the duration of the seismic cycle. This value is highly dependent on the frequency of large flow events allowing efficient transport of sedimentary grain size, and increases with the median grain size. Croissant et al (2017a) take advantage of the conceptual framework of Yanites et al (2010), but develop a numerical model taking into account 2D resolution of hydraulic discharges, vertical and lateral erosion and sediment transport to study the duration of sediment export from a landslide (see Figure 2.5). Above all, the sediment transport capacity Q_T of the river is free to adjust to the geometry of the river, itself modified by erosion and sedimentation processes. This addition is particularly important, as Croissant et al. (2017a) demonstrate that rivers incise landslide deposits by forming a relatively narrow alluvial channel that concentrates the flow, greatly increasing the river's transport capacity and thus reducing sediment removal time to a few years or decades. This effect is even more marked when the volume of the landslide is large or when the initial transport capacity (i.e. before the landslide) of the river is low. It is also important to note that the models of Croissant et al. (2017a) predict a rapid evacuation of sediments while the landslide represents a morphological disturbance for the river. However, given that the sediment transport capacity of the river decreases during the evacuation of sediments and the re-widening of its channel, the evacuation of the remaining sediments falls back on an export dynamics close to Yanites et al. (2010) with a duration of around a few tens to hundreds of years.

An export time, for most sediments, of a few decades instead of a few hundred years has strong implications for post-seismic geomorphological dynamics. Indeed, a duration of a few hundred years implies that river activity during the seismic cycle is mainly limited to evacuating the sediment and eroding its alluvial cover, without allowing a phase of erosion of the rocky bottom. A duration of a few decades, less than or equal to the duration of the seismic cycle, suggests the possibility of a phase of re-incision of the valleys, allowing in turn the hillslopes to redevelop a significant proportion of unstable slopes, before the next major earthquake occurs. This difference in duration also leads to 1) a difference in interpretation between the formation of geomorphological markers, particularly rocky (i.e. strath) or alluvial terraces, and the seismic cycle (Yanites et al., 2010), and 2) a difference in temporality for hazards and hydro-sedimentary risks induced by the sedimentary pulse, which can lead to lateral mobility, avulsion of river channels and flooding (Croissant et al., 2017b). In addition, it is important to note that a major uncertainty remains about the initial state of connectivity of landslide-generated sediments to the river system. Several studies suggest that this initial state of connectivity of the sediments to the river ranges from 8%, with most of the sediments deposited on the hillslopes, to almost 100% (Dadson et al., 2004; Li et al., 2016; West et al., 2011). Moreover, landslide sediments deposited on hillslopes can be remobilized by surface flow during future landslides, debris avalanches, and other gravity processes (Zhang et al., 2019; Fan et al., 2018). These processes control the effectiveness of sediment dynamic connectivity to the river network. The post-seismic sediment export time is therefore the sum of the duration of the dynamic connectivity phase along the hillslopes and the sediment transport phase by river transport (see Figure 2.6). Croissant et al (2019) thus show that the sediment transport dynamics for the New Zealand Alps would, following a scenario for the expected future high magnitude earthquake on the Alpine fault, be limited by the time of connection of landslide sediments to rivers and not by river transport (see Figure 2.6).

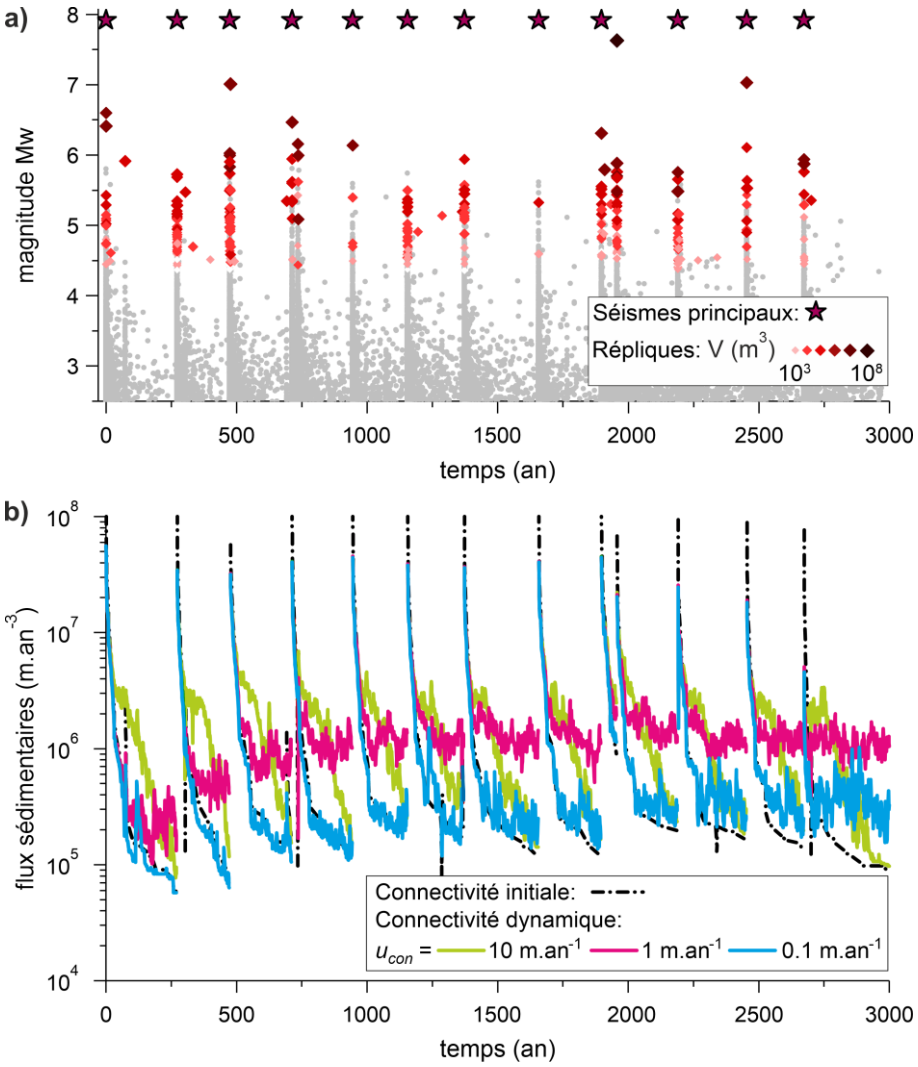

Figure 2.6. *Evolution of sediment flux from co-seismic landslides over several seismic cycles, modified from Croissant et al. (2019). a) Time series of major earthquakes (red stars) and their aftershocks (grey dots), possibly generating a total volume of landslides indicated by colour-coding (diamonds), stochastically modelled by Croissant et al. (2019). The scenario is based on the seismogenic dynamics of the Alpine Fault in New Zealand. b) Temporal evolution of sediment fluxes according to four scenarios of landslide connectivity to rivers: no dynamic connectivity (black dashed line), a dynamic connectivity of 10 (green line), 1 (purple line), and 0.1 m.yr^{-1} (blue line).*

However, the induced post-seismic geomorphological disturbance is not limited to increased sedimentary fluxes. It is observed that debris flows are more likely to be triggered (i.e. for a lower daily precipitation threshold) in the years following a major earthquake (Lin et al., 2004; Zhang & Zhang, 2017; Fan et al., 2019), possibly due to the presence of easily mobilised sediments along the hillslopes. In addition, the number of landslides triggered after a major earthquake is also abnormally high (Marc et al. 2015; Fan et al., 2019). This anomaly is certainly partially amplified by the occurrence of intense rainfall events, but seems to diminish over a period of 1 to 4 years after the earthquake. In addition to the possible impact of rainfall or aftershocks, post-seismic mechanical weakening of the hillslopes, particularly through damage and fracturing triggered during the earthquake, seems to be the main mechanism involved (Marc et al., 2015). This state of transient mechanical weakness is consistent with the observation of subsurface attenuation of seismic wave propagation velocity following a high magnitude earthquake (Brenguier et al., 2008), although the depths considered differ.

Last, the post-seismic geomorphological phase is also characterised by the dynamics of the retreat of knickpoints, formed co-seismically along the trace of the ruptured fault. The height of these co-seismic knickpoints can reach several metres high (e.g., Yanites et al., 2010) and their retreat rate, averaged over several thousand years, is observed to range between about 1 $mm.yr^{-1}$ and 1 $m.yr^{-1}$ (e.g., Van Heijst and Postma, 2001). Co-seismic knickpoints are thus generally considered as geomorphological objects relevant for landscape dynamics on large time scales beyond the duration of a seismic cycle. However, more recent results document retreat rates potentially reaching ~100 $m.yr^{-1}$ over a few years (Yanites et al., 2010; Cook et al., 2013), favoured in particular by the frequency of high water flow events and the presence of bedload sediments (Cook et al., 2013). Such velocities qualify co-seismic knickpoints as fundamental geomorphological objects for understanding landscape dynamics at the scale of a seismic cycle, particularly upstream of faults (Yanites et al., 2010). However, the propagation during the seismic cycle of co-seismic knickpoints and their interaction with the alluvial cover remain poorly understood, despite recent works (Carretier & Lucazeau, 2005; Finnegan & Balco, 2013; Scheingross & Lamb, 2017; Malatesta & Lamb, 2018; Steer et al., 2019).

2.5. Discussions: topographic budget of earthquakes and the seismic cycle

It is now well established, thanks to field observations and semi-empirical models, that the total volume of co-seismic landslides in an active mountain range increases non-linearly with the seismic moment M_0 (Keefer, 1984; Marc et al., 2016a; Croissant

et al., 2019). This result should be related to the quasi-linear increase in the volume of uplifted rocks by co-seismic displacement (Okada, 1985; Marc et al., 2016b; Croissant et al., 2019). A comparison between the volume of co-seismically uplifted rocks and the total volume of co-seismic landslides makes it possible to infer the topographic budget of an earthquake. For example, the 2008 Wenchuan (China) earthquake of magnitude 7.9 triggered ~2.8 km^3 of landslides for ~2.6 km^3 of raised rock volume (Li et al., 2014). Assuming that landslide-driven sediments are evacuated over a duration shorter than the seismic cycle, the topographic budget of the Wenchuan earthquake could be considered as almost neutral. A systematic comparison between the volume of landslides and the volume of uplifted rock suggests that earthquakes of magnitude between 6 and 7.3 can potentially be topographically destructive, or have a neutral budget (Marc et al., 2016b). In other words, these earthquakes of intermediate magnitude do not contribute to the relief building of mountain ranges. Such behaviour is theoretically only possible for a relief with relatively steep modal slopes (>30°) and/or a shallow depth for earthquake nucleation (< 10 km). Earthquakes of magnitude less than ~6 induce PGAs that are too weak to generate a high spatial density of landslides. Earthquakes of magnitude greater than 7 have PGAs that saturate, and the total landslide volume increases less than linearly with M_0, and thus increases less rapidly with M_0 than the volume of uplifted rock. We invite the reader to refer to Marc et al (2016a) and Li et al (2019) for more details on the topographic budget of earthquakes.

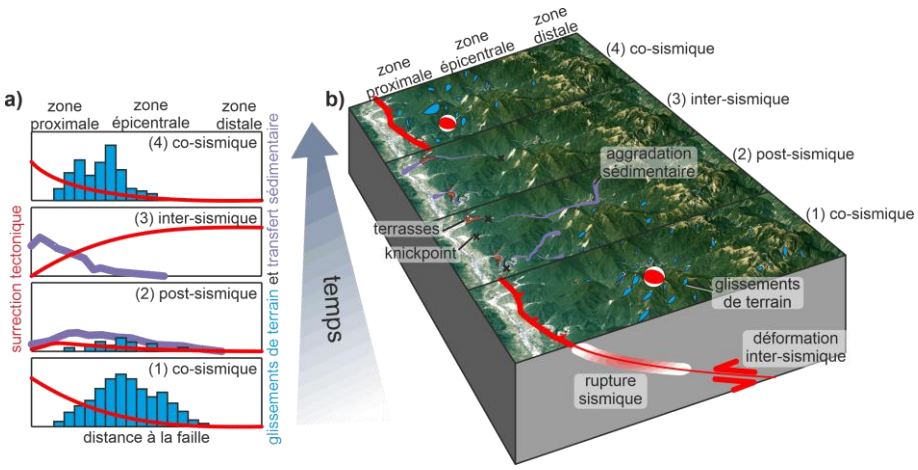

Figure 2.7. *Schematic scheme describing the spatio-temporal evolution of landscapes during the seismic cycle. a) Evolution in profile of tectonic uplift (red), of the number of landslides (histogram in blue) and of the induced sedimentary pulse during the co-, post- and interseismic phases (from bottom to top). b) Evolution in*

map of landscape dynamics and of the tectonic and geomorphological processes related to panel a) during the seismic cycle.

While the impact of earthquakes on the evolution of landscapes during the co- and post-seismic phases has been well studied, particularly following the Chi-Chi and Wenchuan earthquakes, the geomorphological impact of earthquakes on the whole seismic cycle remains relatively poorly known. Although data are lacking, conceptual and numerical models suggest that the geomorphological perturbations induced directly (e.g. landslides, knickpoints) and indirectly (e.g. sedimentary aggradation, high sediment fluxes) by large magnitude earthquakes can control all or part of the landscape dynamics at the scale of the seismic cycle (Yanites et al., 2010; Croissant et al., 2019). However, the frequency of high magnitude earthquakes, the interseismic distribution of tectonic displacements, climatic conditions, variability of hydrological discharges, lithology, drainage density and the state of equilibrium of the landscape are all – probably first order - factors whose role remains largely unexplored. The principle of a landscape at steady-state, with a balance between the rates of erosion and uplift, needs to be reconsidered due to the amplitude and variability of tectonic and geomorphological processes during the seismic cycle. However, it is possible that the landscape may develop a morphological state that allows it (i) to produce an average rate of erosion that is spatially balanced over the long term (t >> seismic cycle) with the uplift rate, and (ii) to digest the geomorphological disturbances induced by large earthquakes in a duration of less than one seismic cycle. A necessary condition for the achievement of this last point (ii) is 1) the evacuation of a significant part of the sediments mobilised by the co-seismic landslides during a seismic cycle allowing 2) rivers to incise their bedrock, 3) to redevelop the slope and height of surrounding hillslopes, destabilised during the previous earthquake, and 4) to recover the potential for triggering new landslides during the next major earthquake, at the beginning of the future seismic cycle (see figure 2.7). To maintain a long-term steady-state and condition (i), the spatial distributions of co-, post- and interseismic uplift must be compensated by equivalent erosion of rivers and hillslopes. We have not mentioned the role of horizontal tectonic displacement that is largely ignored in the literature despite probably having a first order influence on landscape dynamics.

Despite the variability of natural systems and the large uncertainties concerning the dynamics of landscapes during the seismic cycle, we depict here a quantitative and qualitative view of the topographic budget of earthquakes and the seismic cycle (see Figure 2.7). On the hanging wall of the thrust fault, co-seismic uplift generally increases with proximity to the trace of the fault (proximal zone), whereas interseismic uplift increases with distance to the fault (distal zone) (e.g. Cattin & Avouac, 2000). Moreover, the spatial density of co-seismic landslides is generally highest at the epicentre (Meunier et al., 2007), in a transition zone (epicentral zone) between the

proximal and distal zones. The re-incision of rivers in the proximal zone is probably favoured by the presence of co-seismic knickpoints that can rapidly migrate upstream (e.g. Yanites et al., 2010), notably favoured by the increase in post-seismic sedimentary discharge (Cook et al., 2013). This suggests a re-incision of rivers in the proximal part of the river on a scale of a few decades after the earthquake (Yanites et al., 2010). In the distal and epicentral zones, the incision can only start again after the evacuation of the sedimentary input from the co-seismic landslides. The time scales involved are probably a few tens to hundreds of years after the earthquake (Yanites et al., 2010; Croissant et al., 2017) and thus corresponds well to the interseismic phase. However, in order to maintain such a condition, rivers in the epicentral zone must have a higher sediment transport capacity than in the distal zone, as they are subject to a higher spatial density of landslides and additionally receive the products of sediment transport from the distal zone. This increase in transport capacity can occur either 1) permanently, due to the geometric properties of the river bed, as suggested for example for the Peikang River in the epicentral zone of the Chi-Chi earthquake (Yanites et al., 2010), or 2) dynamically by a morphodynamic feedback in response to the abrupt sediment input following the earthquake (Croissant et al., 2017). Thus maintaining a rate of river incision rate balanced with the uplift rate over the entire catchment area is possibly achieved by two quite distinct mechanisms: on the one hand the upstream migration of the co-seismic knickpoints and subsequent incision waves in the zone proximal to the fault, and on the other hand the downstream evacuation of sediments from the landslides in the epicentral and distal zones, allowing a gradual return to detachment-limited conditions (Yanites et al., 2010). For hillslopes, the high density of landslides in the epicentral zone contrasts with the low density generally observed in the distal and proximal zones (Meunier et al., 2007). The paradigm of a topography in a state of dynamic equilibrium thus implies that major earthquakes are not necessarily the trigger for landslides and hillslope erosion in the distal and proximal zones. In the proximal zone, landslides triggered by frequent earthquakes of moderate magnitude and shallow depth could partially compensate for this erosion deficit. Whereas in the distal zone, landslides not triggered by earthquakes or triggered by heavy rainfall events and other erosion processes (e.g. soil creeping) could dominate hillslope dynamics. But such hypothetical scenarios imply close relationships, still poorly understood, between 1) the organization of landscapes, built on geological time scales (10 kan-10 Ma), and 2) the capacity of these landforms to respond to disturbances on a time scale of a few tens or hundreds of years, shorter than the return time of these disturbances. Numerical modelling of geomorphological and tectonic processes during the seismic cycle thus offers a unique approach to understanding how landscapes behave on these different time scales.

2.6. Prospects: impact of erosion on fault and earthquake dynamics

Acknowledging the role of extreme events and the high variability of short-scale erosion rates on landscape dynamics has implications that go beyond purely geomorphological considerations. Indeed, numerical models, coupling tectonic deformation and erosion processes on geological time scales (1-10 Myr), suggest that the spatial distribution of erosion significantly impacts the distribution and intensity of tectonic deformation in mountain ranges (e.g. Willett et al., 1999; Thieulot et al., 2014). On intermediate time scales (10 kyr - 1 Myr), erosion and induced isostatic rebound can promote sliding along certain faults (Calais et al., 2010; Vernant et al., 2013). At the scale of the seismic cycle (<1000 yr), erosion and induced mass unloading at the surface may contribute to elastically load stresses on underlying thrust faults (see Figure 2.8; Steer et al., 2014). This effect is all the more marked at shallow depths (< 5 km), since the static Coulomb stress ΔCFF induced by surface erosion, evaluated at depth z, has an amplitude that decreases in z^{-2}. Moreover, for a point unload F, the change in ΔCFF is directly proportional to the value of F and thus increases linearly with the amount of erosion. It is also important to point out that erosion, unlike other external forcings with a certain periodicity (i.e. hydrological load or tidal effect), generates a temporal accumulation of stresses on a fault plane in an elastic environment at the scale of the seismic cycle.

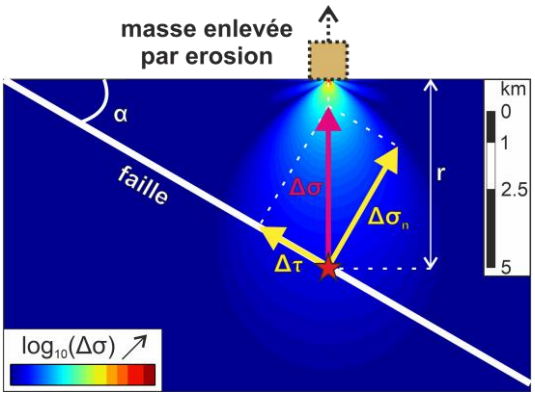

Figure 2.8. *Schematic scheme illustrating the spatial distribution of the stress increment Δσ (here purely illustrative) induced by surface point erosion, increasing both the tangential stress Δτ and the normal stress $\Delta\sigma_n$. Modified from Steer et al (2014).*

Steer et al. (2014) suggest that such dependence of the stress state of the faults on the spatial and temporal distribution of surface erosion is favourable for the

occurrence of shallow earthquakes triggered by erosion. Steer et al. (2014) proposes two particularly favourable cases: 1) extreme events, such as large magnitude earthquakes and intense rainfall events, triggering a large volume of landslides and rapid export of sediments, and 2) the extraction of large volumes of rock from quarries. For example, the magnitude 5 Teil earthquake (southern France) of 11 November 2019, with a rupture fault plane located between the surface and about 1.5 km of depth, could have been triggered by the extraction of rock from a quarry located just above the rupture fault. In this particular case, the ~0.03 km3 of rock extracted from the quarry between 1946 and 2019 could have induced a ΔCFF around 1.5 to 2 bar, compared with the stress drop induced by the earthquake, possibly around 10 bar. Moreover, quasi-dynamic numerical models of the seismic cycle, considering frictional faults following a rate-and-state law, suggest that variations in normal stresses induced by surface erosion can affect seismicity (Jeandet-Ribes et al., 2020). More specifically, a rapid variation, i.e. shorter than the duration of the seismic cycle, of the normal stress can lead to more frequent earthquakes associated with lower magnitudes (i.e. a higher b-value for the Gutenberg-Richter law). Taking advantage of theoretical frameworks, (Steer et al., 2020) demonstrate that the frequency of shallow earthquakes in Taiwan increased for 2.5 years following Typhoon Morakot in 2009, which triggered a large number of landslides, corresponding to a volume of 1.2 km^3 , and a relatively rapid and intense erosion of the landscape. Such results illustrate once again the need to better constrain sedimentary evacuation after a geomorphological disturbance triggered by a major earthquake or intense rainfall event.

2.7. References

[AHN 70] AHNERT, F., Functional relationships between denudation, relief, and uplift in large, mid-latitude drainage basins. American Journal of Science, 268(3), 243-263, 1970.

[BAR 12] BARLOW, J., LIM, M., ROSSER, N., PETLEY, D., BRAIN, M., NORMAN, E., & GEER, M., Modeling cliff erosion using negative power law scaling of rockfalls. Geomorphology, 139, 416-424, 2012.

[BER 20] BERNARD, T., LAGUE, D., & STEER, P., 3D point cloud LiDAR differencing method apply to region scale landslide detection and volume estimation: Application to the Kaikoura region, New Zealand. Earth Surface Dynamics, submitted, 2020.

[BON 03] BONNET, S., & CRAVE, A., Landscape response to climate change: Insights from experimental modeling and implications for tectonic versus climatic uplift of topography. Geology, 31(2), 123-126, 2003

[BOO 08] BOORE, D. M., & ATKINSON, G. M., Ground-motion prediction equations for the average horizontal component of PGA, PGV, and 5%-damped PSA at spectral periods between 0.01 s and 10.0 s. Earthquake Spectra, 24(1), 99-138, 2008.

[BRA 13] BRAUN, J., & WILLETT, S. D., A very efficient O (n), implicit and parallel method to solve the stream power equation governing fluvial incision and landscape evolution. Geomorphology, 180, 170-179, 2013.

[BRE 08] BRENGUIER, F., CAMPILLO, M., HADZIIOANNOU, C., SHAPIRO, N. M., NADEAU, R. M., & LAROSE, E., Postseismic relaxation along the San Andreas fault at Parkfield from continuous seismological observations. science, 321(5895), 1478-1481, 2008.

[CAL 10] CALAIS, E., FREED, A. M., VAN ARSDALE, R., & STEIN, S., Triggering of New Madrid seismicity by late-Pleistocene erosion. Nature, 466(7306), 608-611, 2010.

[CAM 17] CAMPFORTS, B., SCHWANGHART, W., & GOVERS, G., Accurate simulation of transient landscape evolution by eliminating numerical diffusion: the TTLEM 1.0 model. Earth Surface Dynamics, 5(1), 47-66, 2017.

[CAR 05] CARRETIER, S., & LUCAZEAU, F., How does alluvial sedimentation at range fronts modify the erosional dynamics of mountain catchments?. Basin research, 17(3), 361-381, 2005.

[CAT 00] CATTIN, R., & AVOUAC, J. P., Modeling mountain building and the seismic cycle in the Himalaya of Nepal. Journal of Geophysical Research: Solid Earth, 105(B6), 13389-13407, 2000.

[COOK 13] COOK, K. L., TUROWSKI, J. M., & HOVIUS, N., A demonstration of the importance of bedload transport for fluvial bedrock erosion and knickpoint propagation. Earth Surface Processes and Landforms, 38(7), 683-695, 2013.

[CRA 01] CRAVE, A., & DAVY, P., A stochastic "precipiton" model for simulating erosion/sedimentation dynamics. Computers & Geosciences, 27(7), 815-827, 2001.

[CRO 17a] CROISSANT, T., LAGUE, D., STEER, P., & DAVY, P., Rapid post-seismic landslide evacuation boosted by dynamic river width. Nature Geoscience, 10(9), 680-684, 2017a.

[CRO 17b] CROISSANT, T., LAGUE, D., DAVY, P., DAVIES, T., & STEER, P., A precipiton-based approach to model hydro-sedimentary hazards induced by large sediment supplies in alluvial fans. Earth Surface Processes and Landforms, 42(13), 2054-2067, 2017b.

[CRO 19] CROISSANT, T., STEER, P., LAGUE, D., DAVY, P., JEANDET, L., & HILTON, R. G., Seismic cycles, earthquakes, landslides and sediment fluxes: Linking tectonics to surface processes using a reduced-complexity model. Geomorphology, 339, 87-103, 2019.

[DAD 13] DADSON, S. J., HOVIUS, N., CHEN, H., DADE, W. B., HSIEH, M. L., WILLETT, S. D., ... & LAGUE, D., Links between erosion, runoff variability and seismicity in the Taiwan orogen. Nature, 426(6967), 648-651, 2003.

[DAD 14] DADSON, S. J., HOVIUS, N., CHEN, H., DADE, W. B., LIN, J. C., HSU, M. L., ... & STARK, C. P., Earthquake-triggered increase in sediment delivery from an active mountain belt. Geology, 32(8), 733-736, 2004.

[DAVY 17] DAVY, P., CROISSANT, T., & LAGUE, D., A precipiton method to calculate river hydrodynamics, with applications to flood prediction, landscape evolution models, and braiding instabilities. Journal of geophysical research: earth surface, 122(8), 1491-1512, 2017.

[EMB 16] EMBERSON, R., HOVIUS, N., GALY, A., & MARC, O., Chemical weathering in active mountain belts controlled by stochastic bedrock landsliding. Nature Geoscience, 9(1), 42-45, 2016.

[FAN 18] FAN, X., JUANG, C. H., WASOWSKI, J., HUANG, R., XU, Q., SCARINGI, G., ... & HAVENITH, H. B., What we have learned from the 2008 Wenchuan Earthquake and its aftermath: A decade of research and challenges. Engineering geology, 241, 25-32, 2018.

[FAN 19] FAN, X., SCARINGI, G., KORUP, O., WEST, A. J., VAN WESTEN, C. J., TANYAS, H., ... & ZHANG, L., Earthquake-induced chains of geologic hazards: Patterns, mechanisms, and impacts. Reviews of geophysics, 57(2), 421-503, 2019.

[FIN 13] FINNEGAN, N. J., & BALCO, G., Sediment supply, base level, braiding, and bedrock river terrace formation: Arroyo Seco, California, USA. Bulletin, 125(7-8), 1114-1124, 2013.

[FIN 14] FINNEGAN, N. J., SCHUMER, R., & FINNEGAN, S., A signature of transience in bedrock river incision rates over timescales of 10 4–10 7 years. Nature, 505(7483), 391-394, 2014.

[FRI 18] FRITH, N. V., HILTON, R. G., HOWARTH, J. D., GRÖCKE, D. R., FITZSIMONS, S. J., CROISSANT, T., ... & DENSMORE, A. L., Carbon export from mountain forests enhanced by earthquake-triggered landslides over millennia. Nature Geoscience, 11(10), 772-776, 2018.

[GIL 77] GILBERT, G. K., Report on the Geology of the Henry Mountains, Dept. of the Interior, US Geographical and Geological Survey of the Rocky Mountain Region, Washington, D.C., 1877.

[GUZ 02] GUZZETTI, F., MALAMUD, B. D., TURCOTTE, D. L., & REICHENBACH, P., Power-law correlations of landslide areas in central Italy. Earth and Planetary Science Letters, 195(3-4), 169-183, 2002.

[HIL 08] HILTON, R. G., GALY, A., HOVIUS, N., CHEN, M. C., HORNG, M. J., & CHEN, H., Tropical-cyclone-driven erosion of the terrestrial biosphere from mountains. Nature Geoscience, 1(11), 759-762, 2008.

[HOV 11] HOVIUS, N., MEUNIER, P., LIN, C. W., CHEN, H., CHEN, Y. G., DADSON, S., ... & LINES, M., Prolonged seismically induced erosion and the mass balance of a large earthquake. Earth and Planetary Science Letters, 304(3-4), 347-355, 2011.

[HOW 83] HOWARD, A. D., & KERBY, G., Channel changes in badlands. Geological Society of America Bulletin, 94(6), 739-752, 1983.

[HOW 94] HOWARD, A. D., DIETRICH, W. E., & SEIDL, M. A., Modeling fluvial erosion on regional to continental scales. Journal of Geophysical Research: Solid Earth, 99(B7), 13971-13986, 1994.

[HOW 12] HOWARTH, J. D., FITZSIMONS, S. J., NORRIS, R. J., & JACOBSEN, G. E., Lake sediments record cycles of sediment flux driven by large earthquakes on the Alpine fault, New Zealand. Geology, 40(12), 1091-1094, 2012.

[HOW 14] HOWARTH, J. D., FITZSIMONS, S. J., NORRIS, R. J., & JACOBSEN, G. E., Lake sediments record high intensity shaking that provides insight into the location and rupture length of large earthquakes on the Alpine Fault, New Zealand. Earth and Planetary Science Letters, 403, 340-351, 2014.

[HUA 13] HUANG, M. Y. F., & MONTGOMERY, D. R., Altered regional sediment transport regime after a large typhoon, southern Taiwan. Geology, 41(12), 1223-1226, 2013.

[JEA 19] JEANDET, L., STEER, P., LAGUE, D., & DAVY, P., Coulomb mechanics and relief constraints explain landslide size distribution. Geophysical Research Letters, 46(8), 4258-4266, 2019.

[JEA 20] JEANDET RIBES, L., CUBAS, N., BHAT, H., & STEER. P., The impact of large erosional events and transient normal stress changes on the seismicity of faults. Geophysical Research Letters, submitted, 2020.

[JEA 18] JEANDET, L., Modélisation numérique des liens entre séismes et glissements de terrain au cours du cycle sismique: processus déclencheurs, distributions de tailles et implications géologiques, Doctoral dissertation, Université Rennes 1, 2018.

[KEE 84] KEEFER, D. K., Landslides caused by earthquakes. Geological Society of America Bulletin, 95(4), 406-421, 1984.

[KEE 99] KEEFER, D. K., Earthquake-induced landslides and their effects on alluvial fans. Journal of Sedimentary Research, 69(1), 84-104, 1999.

[KIR 12] KIRBY, E., & WHIPPLE, K. X., Expression of active tectonics in erosional landscapes. Journal of Structural Geology, 44, 54-75, 2012.

[LAG 05] LAGUE, D., HOVIUS, N., & DAVY, P., Discharge, discharge variability, and the bedrock channel profile. Journal of Geophysical Research: Earth Surface, 110(F4), 2005.

[LAG 14] LAGUE, D., The stream power river incision model: evidence, theory and beyond. Earth Surface Processes and Landforms, 39(1), 38-61, 2014.

[LAR 10] LARSEN, I. J., MONTGOMERY, D. R., & KORUP, O., Landslide erosion controlled by hillslope material. Nature Geoscience, 3(4), 247-251, 2010.

[LEO 10] LEONARD, M., Earthquake fault scaling: Self-consistent relating of rupture length, width, average displacement, and moment release. Bulletin of the Seismological Society of America, 100(5A), 1971-1988, 2010.

[LI 14] LI, G., WEST, A. J., DENSMORE, A. L., JIN, Z., PARKER, R. N., & HILTON, R. G., Seismic mountain building: Landslides associated with the 2008 Wenchuan earthquake in the context of a generalized model for earthquake volume balance. Geochemistry, Geophysics, Geosystems, 15(4), 833-844, 2014.

[LI 16] LI, G., WEST, A. J., DENSMORE, A. L., HAMMOND, D. E., JIN, Z., ZHANG, F., ... & HILTON, R. G., Connectivity of earthquake-triggered landslides with the fluvial network: Implications for landslide sediment transport after the 2008 Wenchuan earthquake. Journal of Geophysical Research: Earth Surface, 121(4), 703-724, 2016.

[LI 19] LI, G., WEST, A. J., & QIU, H., Competing effects of mountain uplift and landslide erosion over earthquake cycles. Journal of Geophysical Research: Solid Earth, 124(5), 5101-5133, 2019.

[LIN 04] LIN, C. W., SHIEH, C. L., YUAN, B. D., SHIEH, Y. C., LIU, S. H., & LEE, S. Y., Impact of Chi-Chi earthquake on the occurrence of landslides and debris flows: example from the Chenyulan River watershed, Nantou, Taiwan. Engineering geology, 71(1-2), 49-61, 2004.

[LIN 11] LIN, C. W., CHANG, W. S., LIU, S. H., TSAI, T. T., LEE, S. P., TSANG, Y. C., ... & TSENG, C. M., Landslides triggered by the 7 August 2009 Typhoon Morakot in southern Taiwan. Engineering Geology, 123(1-2), 3-12, 2011.

[MAL 04] MALAMUD, B. D., TURCOTTE, D. L., GUZZETTI, F., & REICHENBACH, P., Landslide inventories and their statistical properties. Earth Surface Processes and Landforms, 29(6), 687-711, 2004.

[MAL 18] MALATESTA, L. C., & LAMB, M. P., Formation of waterfalls by intermittent burial of active faults. GSA Bulletin, 130(3-4), 522-536, 2018.

[MAR 15a] MARC, O., & HOVIUS, N., Amalgamation in landslide maps: effects and automatic detection. Natural Hazards & Earth System Sciences, 15(4), 2015.

[MAR 15b] MARC, O., HOVIUS, N., MEUNIER, P., UCHIDA, T., & HAYASHI, S., Transient changes of landslide rates after earthquakes. Geology, 43(10), 883-886, 2015.

[MAR 16a] MARC, O., HOVIUS, N., & MEUNIER, P., The mass balance of earthquakes and earthquake sequences. Geophysical Research Letters, 43(8), 3708-3716, 2016a.

[MAR 16b] MARC, O., HOVIUS, N., MEUNIER, P., GORUM, T., & UCHIDA, T., A seismologically consistent expression for the total area and volume of earthquake-triggered landsliding. Journal of Geophysical Research: Earth Surface, 121(4), 640-663, 2016b.

[MAR 18] MARC, O., STUMPF, A., MALET, J. P., GOSSET, M., UCHIDA, T., & CHIANG, S. H., Initial insights from a global database of rainfall-induced landslide inventories: the weak influence of slope and strong influence of total storm rainfall. Earth Surface Dynamics, 6(4), 2018.

[MAS 18] MASSEY, C., TOWNSEND, D., RATHJE, E., ALLSTADT, K. E., LUKOVIC, B., KANEKO, Y., ... & HORSPOOL, N., Landslides Triggered by the 14 November 2016 Mw 7.8 Kaikōura Earthquake, New ZealandLandslides Triggered by the 14 November 2016 Mw 7.8 Kaikōura Earthquake, New Zealand. Bulletin of the Seismological Society of America, 108(3B), 1630-1648, 2018.

[MAT 53] MATHUR, L. P., Assam earthquake of 15th August 1950—a short note on factual observations In A compilation of papers on the Assam earthquake of August 15, 1950 (ed. Rao, MBR) Vol. National Geophysical Research Institute, Hyperabad, India, 56-60, 1953.

[MEU 07] MEUNIER, P., HOVIUS, N., & HAINES, A. J., Regional patterns of earthquake-triggered landslides and their relation to ground motion. Geophysical Research Letters, 34(20), 2007.

[MIL 13] MILLIMAN, J. D., & FARNSWORTH, K. L., River discharge to the coastal ocean: a global synthesis. Cambridge University Press, 2013.

[MOHR 17] MOHR, C. H., MANGA, M., WANG, C. Y., & KORUP, O., Regional changes in streamflow after a megathrust earthquake. Earth and Planetary Science Letters, 458, 418-428, 2017.

[MON 03] MONTGOMERY, D. R., & MANGA, M., Streamflow and water well responses to earthquakes. Science, 300(5628), 2047-2049, 2003.

[NEW 65] NEWMARK, N. M., Effects of earthquakes on dams and embankments. Geotechnique, 15(2), 139-160, 1965.

[OKA 85] OKADA, Y., Surface deformation due to shear and tensile faults in a half-space. Bulletin of the seismological society of America, 75(4), 1135-1154, 1985.

[PAR 11] PARKER, R. N., DENSMORE, A. L., ROSSER, N. J., DE MICHELE, M., LI, Y., HUANG, R., ... & PETLEY, D. N., Mass wasting triggered by the 2008 Wenchuan earthquake is greater than orogenic growth. Nature Geoscience, 4(7), 449-452, 2011.

[PEI 01] PEIZHEN, Z., MOLNAR, P., & DOWNS, W. R., Increased sedimentation rates and grain sizes 2–4 Myr ago due to the influence of climate change on erosion rates. Nature, 410(6831), 891-897, 2001.

[SCH 17] SCHEINGROSS, J. S., & LAMB, M. P., A mechanistic model of waterfall plunge pool erosion into bedrock. Journal of Geophysical Research: Earth Surface, 122(11), 2079-2104, 2017.

[SCH 97] SCHOLZ, C. H., Size distributions for large and small earthquakes. Bulletin of the Seismological Society of America, 87(4), 1074-1077, 1997.

[SIM 67] SIMONETT, D. S., Landslide distribution and earthquakes in the Bavani and Torricelli Mountains, New Guinea. Landform Studies from Australia and New Guinea, 64-84, 1967.

[STA 01] STARK, C. P., & HOVIUS, N., The characterization of landslide size distributions. Geophysical Research Letters, 28(6), 1091-1094, 2001.

[STE 14] STEER, P., SIMOES, M., CATTIN, R., & SHYU, J. B. H., Erosion influences the seismicity of active thrust faults. Nature communications, 5(1), 1-7, 2014.

[STE 19] STEER, P., CROISSANT, T., BAYNES, E., & LAGUE, D., Statistical modelling of co-seismic knickpoint formation and river response to fault slip. Earth surface dynamics., 7(3), 681-706, 2019.

[TAN 17] TANYAŞ, H., VAN WESTEN, C. J., ALLSTADT, K. E., ANNA NOWICKI JESSEE, M., GÖRÜM, T., JIBSON, R. W., ... & HOVIUS, N., Presentation and analysis of a worldwide database of earthquake-induced landslide inventories. Journal of Geophysical Research: Earth Surface, 122(10), 1991-2015, 2017.

[TAN 19] TANYAŞ, H., VAN WESTEN, C. J., ALLSTADT, K. E., & JIBSON, R. W., Factors controlling landslide frequency–area distributions. Earth surface processes and landforms, 44(4), 900-917, 2019.

[TEB 20] TEBBENS, S. F., Landslide scaling: A review. Earth and Space Science, 7(1), e2019EA000662, 2020.

[THI 14] THIEULOT, C., STEER, P., & HUISMANS, R. S., Three-dimensional numerical simulations of crustal systems undergoing orogeny and subjected to surface processes. Geochemistry, Geophysics, Geosystems, 15(12), 4936-4957, 2014.

[TUC 01] TUCKER, G. E., LANCASTER, S. T., GASPARINI, N. M., BRAS, R. L., & RYBARCZYK, S. M., An object-oriented framework for distributed hydrologic and geomorphic modeling using triangulated irregular networks. Computers & Geosciences, 27(8), 959-973, 2001.

[VAN 07] VAN DEN EECKHAUT, M., POESEN, J., GOVERS, G., VERSTRAETEN, G., & DEMOULIN, A., Characteristics of the size distribution of recent and historical landslides in a populated hilly region. Earth and Planetary Science Letters, 256(3-4), 588-603, 2007.

[VAN 01] VAN HEIJST, M. W. I. M., & POSTMA, G., Fluvial response to sea-level changes: a quantitative analogue, experimental approach. Basin Research, 13(3), 269-292, 2001.

[VER 13] VERNANT, P., HIVERT, F., CHERY, J., STEER, P., CATTIN, R., & RIGO, A., Erosion-induced isostatic rebound triggers extension in low convergent mountain ranges. Geology, 41(4), 467-470, 2013.

[WAN 15] WANG, J., JIN, Z., HILTON, R. G., ZHANG, F., DENSMORE, A. L., LI, G., & WEST, A. J., Controls on fluvial evacuation of sediment from earthquake-triggered landslides. Geology, 43(2), 115-118, 2015.

[WAN 17] WANG, W., GODARD, V., LIU-ZENG, J., SCHERLER, D., XU, C., ZHANG, J., ... & ASTER TEAM, Perturbation of fluvial sediment fluxes following the 2008 Wenchuan earthquake. Earth Surface Processes and Landforms, 42(15), 2611-2622, 2017.

[WEST 11] WEST, A. J., LIN, C. W., LIN, T. C., HILTON, R. G., LIU, S. H., CHANG, C. T., ... & HOVIUS, N., Mobilization and transport of coarse woody debris to the oceans triggered by an extreme tropical storm. Limnology and oceanography, 56(1), 77-85, 2011.

[WEST 14] WEST, A. J., HETZEL, R., LI, G., JIN, Z., ZHANG, F., HILTON, R. G., & DENSMORE, A. L., Dilution of 10Be in detrital quartz by earthquake-induced landslides: Implications for determining denudation rates and potential to provide insights into landslide sediment dynamics. Earth and Planetary Science Letters, 396, 143-153, 2014.

[WHI 99] WHIPPLE, K. X., & TUCKER, G. E., Dynamics of the stream-power river incision model: Implications for height limits of mountain ranges, landscape response timescales, and research needs. Journal of Geophysical Research: Solid Earth, 104(B8), 17661-17674, 1999.

[WHI 02] WHIPPLE, K. X., & TUCKER, G. E., Implications of sediment-flux-dependent river incision models for landscape evolution. Journal of Geophysical Research: Solid Earth, 107(B2), ETG-3, 2002.

[WHI 01] WHIPPLE, K. X., Fluvial landscape response time: how plausible is steady-state denudation?. American Journal of Science, 301(4-5), 313-325, 2001.

[WHI 09] WHIPPLE, K. X., The influence of climate on the tectonic evolution of mountain belts. Nature geoscience, 2(2), 97-104, 2009.

[WIL 99] WILLETT, S. D., Orogeny and orography: The effects of erosion on the structure of mountain belts. Journal of Geophysical Research: Solid Earth, 104(B12), 28957-28981, 1999.

[WIL 14] WILLETT, S. D., MCCOY, S. W., PERRON, J. T., GOREN, L., & CHEN, C. Y., Dynamic reorganization of river basins. Science, 343(6175), 1248765, 2014.

[WIL 18] WILLIAMS, J. G., ROSSER, N. J., HARDY, R. J., BRAIN, M. J., & AFANA, A. A., Optimising 4-D surface change detection: an approach for capturing rockfall magnitude–frequency. Earth surface dynamics., 6(1), 101-119, 2018.

[YAM 18] YAMAGISHI, H., & YAMAZAKI, F., Landslides by the 2018 Hokkaido Iburi-Tobu Earthquake on September 6. Landslides, 15(12), 2521-2524, 2018.

[YAN 10] YANITES, B. J., TUCKER, G. E., MUELLER, K. J., & CHEN, Y. G., How rivers react to large earthquakes: Evidence from central Taiwan. Geology, 38(7), 639-642, 2010.

[ZHA 17] ZHANG, S., & ZHANG, L. M., Impact of the 2008 Wenchuan earthquake in China on subsequent long-term debris flow activities in the epicentral area. Geomorphology, 276, 86-103, 2017.

[ZHA 19] ZHANG, F., JIN, Z., WEST, A. J., AN, Z., HILTON, R. G., WANG, J., ... & SUN, Y., Monsoonal control on a delayed response of sedimentation to the 2008 Wenchuan earthquake. Science advances, 5(6), eaav7110, 2019.